Spatial coherence of nonlinear dynamics in a semiconductor experiment

Joachim Peinke
Centre de Recherches sur les Très Basses Températures, CNRS, 25 avenue des Martyrs, 166X-Centre de Tri, F-38042 Grenoble CEDEX, France

Reinhard Richter
Physical Institute, University of Tübingen, Morgenstelle 14, W-7400 Tübingen, Germany

Jürgen Parisi
Physics Institute, University of Zurich, Schönberggasse 9, CH-8001 Zurich, Switzerland
(Received 10 February 1992; revised manuscript received 13 July 1992)

For the case of an experimental semiconductor system, it is shown how different dynamical states that range from periodicity to hyperchaos are connected to distinct spatial patterns developing inside the sample. Collective synchronization of subsystems gives rise to low-dimensional periodic states, whereas the interaction of spatially localized oscillation centers leads to quasiperiodicity and ordinary chaos as well as higher-dimensional chaotic dynamics.

I. INTRODUCTION

Nature fascinates us by spontaneously forming structures both in space and time. The challenging question for the basic mechanism bringing about all those structural forms is nowadays attributed to nonlinear spatiotemporal processes. Specifically, investigating total arrays of coupled nonlinear systems, i.e., taking space as a discrete variable, has turned out to represent an elegant and popular method. The separate uncoupled system usually shows behavior described by simple dynamics. The spontaneous formation of more or less complicated patterns in such multicomponent systems is of current interest. One typical result comprises the emergence of coherent clusters of subsystems that exhibit low-dimensional deterministic dynamical behavior (see, for example, Ref. 1). In this case, the multicomponent system becomes locally reducible to a generic dynamics, which is governed only by a few variables.

This paper reports on experimental results from one exemplary semiconductor system, namely, the electric avalanche breakdown of homogeneously doped p-type germanium at low temperatures. In close analogy to the introductory ideas above, we point out the way nonlinear dynamics are caused by the mutual interaction of competitive subsystems inside the semiconductor device. Particular merits of our experimental system are the huge diversity of different nonlinear dynamical phenomena obtained under minute changes of the working conditions. Thus, in an extremely small regime of parameter space, transitions from fixed points to limit cycles, quasiperiodicity, as well as universal routes to chaos and hyperchaos were found.[2–7] To explain the creation of further degrees of freedom as a consequence of the increasing attractor dimensionality, we conjectured a model consisting of many coupled oscillatory subsystems.[3,7–9] Up to now, the following experimental evidence has been delivered for that working hypothesis. First, spatiotemporal dynamics is provided by the self-sustained development of filamentary current structures coinciding with the appearance of spontaneous oscillations. Second, distinguished oscillatory centers are found to be localized at the boundary of the filaments.[10] Third, the location of these oscillators is restricted to distinct finite regions inside the filament boundary,[11] in contrast to other semiconductor systems, where the boundaries of the spatial structures obey a uniform breathing mode.[12] Detection of those space-time patterns was performed via the well-established imaging technique of low-temperature scanning electron microscopy. Since the above method takes into account only the linear response of the system investigated, the understanding of nonlinear dynamics like chaos has still remained an open question. At this point, a different measuring procedure capable of proving the nonlinear interplay between subsystems comes to the rescue, as described in the following.

Our paper is organized as follows. After a short introduction into the basic elements of the experimental system in Sec. II, Sec. III describes the spatial localization of a periodically oscillating center of finite size. Such an oscillator is a result of synchronizing subsystems showing independent dynamics when they are singularized. In Sec. IV, we demonstrate the existence of two spatially separated oscillation centers for the case of a quasiperiodic state. Upon switching one center on and off, one can furnish proof that there, indeed, is a nonlinear interaction among the oscillators present. Furthermore, the development of the spatial interrelation of different sample regions has been analyzed for the case of chaotic dynamics (Sec. V).

II. EXPERIMENT

The experimental system consists of a homogeneously doped p-type germanium sample with ohmic contacts. The concentration of shallow acceptors is about 10^{14}

cm^{-3}, their binding energy about 10 meV. The spectroscopic characterization of the acceptors involved as well as further material details can be found elsewhere.[13] Out of that single-crystalline semiconductor wafer, a sample with the typical dimensions of $5\times2\times0.2$ mm^3 was cut. After passivation of surface states by means of mechanical polishing and subsequent chemical etching, ohmic contact areas were arranged at one of the two largest specimen surfaces. Hereto, either aluminum was evaporated and successively alloyed with the germanium crystal or boron was ion implanted. Both methods gave no significant difference in the electric behavior. In the following, we present results obtained from a sample with aluminum contacts. The arrangement of the contacts together with the experimental setup are shown in Fig. 1. The local probes served to detect partial voltage drops, as will be discussed later on in more detail.

The above sample configuration was mounted in a liquid-helium cryostage. A copper shield provided a careful screening against infrared radiation, which sensitively influences the sample behavior at low temperatures. By the help of a vapor-pressure regulation, the temperature could be varied between 1.7 and 4.2 K. As a further variable external parameter, a magnetic field could be applied. It was oriented perpendicular to the broad side of the sample, i.e., perpendicular to the direction of the electric field inside the sample.

The electric behavior of the above semiconductor material is mainly determined by the reduced thermal energy owing to the low temperatures. There, the charge carriers freeze out at the impurities such that the semiconductor becomes highly insulating. This temperature effect can be inverted through application of an electric field: the few remaining mobile charge carriers are accelerated and, thus, gain kinetic energy. The energy gain increases with increasing electric field, if the mean lifetime of the charge carriers remains constant (corresponding to a constant carrier mobility). When the gain in kinetic energy surpasses the ionization energy of trapped charge carriers, an avalanchelike multiplication of the mobile carriers takes place. This effect is called avalanche breakdown due to impurity impact ionization. In terms of rate equations,[14] we there have an increase of the impact ionization coefficient so that the total generation rate becomes larger than the recombination rate of the mobile charge carriers. So far, avalanche breakdown is a pure electric-field effect. To best verify the quality of the ohmic contacts and also the validity of the model understanding, one checks this field effect upon changing the sample length accordingly. The results of these experiments (reported elsewhere[15]), moreover, tell us that the prevailing breakdown definitely is a bulk effect. Of course, its concrete electric behavior sensitively depends on the actual impurity concentration.[16]

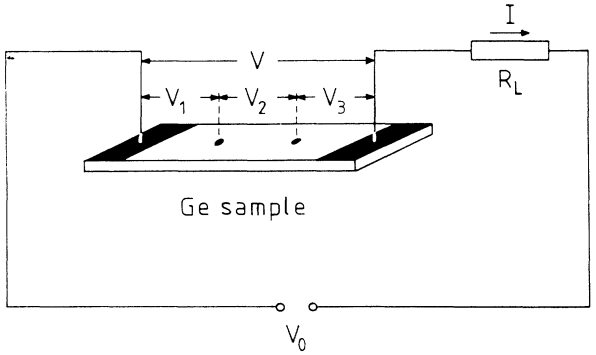

FIG. 1. Scheme of the experimental arrangement applied to the semiconductor sample. The shaded areas on the specimen surface indicate the ohmic contacts.

For the present experimental system, avalanche breakdown takes place at typical electric-field values of 5 V/cm. It manifests in a dramatic increase of the current by more than six orders of magnitude.[17] In the current-voltage characteristic, the breakdown region excels in either hysteretic or negative differential resistance behavior, depending on whether the load resistor applied is small or large, respectively (corresponding to the realization of the two extreme cases of voltage and current control). Just during the above transition from a low to a high conducting state, one discovers a multicolored collection of nonlinear dynamical phenomena.[18] In the following, we concentrate on a particular dynamics governing the immediate postbreakdown regime, the so-called structure-limited oscillations,[19] that take place only when stable current filaments can exist permanently.

III. DYNAMICS OF THE WHOLE MULTICOMPONENT SYSTEM

Let us start with some comments on the experimental setup. The spatial components of the total system dynamics were investigated by means of local contact probes attached to the broad surface of the germanium crystal (see the sample geometry in Fig. 1). A dc bias voltage V_0 supplies the series combination of the sample and the load resistor R_L. In addition to the total voltage V, the partial voltage drops V_i $(i=1,2,3)$ can independently be measured along the sample. They provide spatially localized system answers of the corresponding sample parts. On the other hand, the resulting current I, recorded via the voltage drop at the load resistor, gives the integral whole answer of the semiconductor system. We point out that phase portraits constructed from different partial voltage drops not only reflect a two-dimensional projection of the attractor, but also can be interpreted as direct measurement of the temporal coherence between distinct localized regions of the sample investigated. Say, there were no spatially inhomogeneous dynamics present; the time signals of those partial voltage drops would have to be proportional to each other. Then, the resulting phase portraits would represent no more than a straight line. From this, we conclude that phase portraits of two distinct partial voltage signals displaying any structural difference to a straight line indicate the existence of different dynamical behavior in different spatial regions of the system. The simplest case would be a pure phase shift.

Figure 2 gives a sequence of phase portraits that are constructed from different pairs of partial voltage drops V_i $(i=1,2,3)$. The corresponding dynamics ranges from

a stable fixed point to hyperchaos.[7,8] It immediately becomes obvious how the oscillatory behavior in distinct sample parts gradually decorrelates with increasing degrees of dynamical complexity (i.e., with increasing dimensionality of the overall system). For example, the phase portrait of the periodic state [Fig. 2(b)] has nearly the form of a straight line due to the strong coherence between both partial voltage signals. Note that the sign of

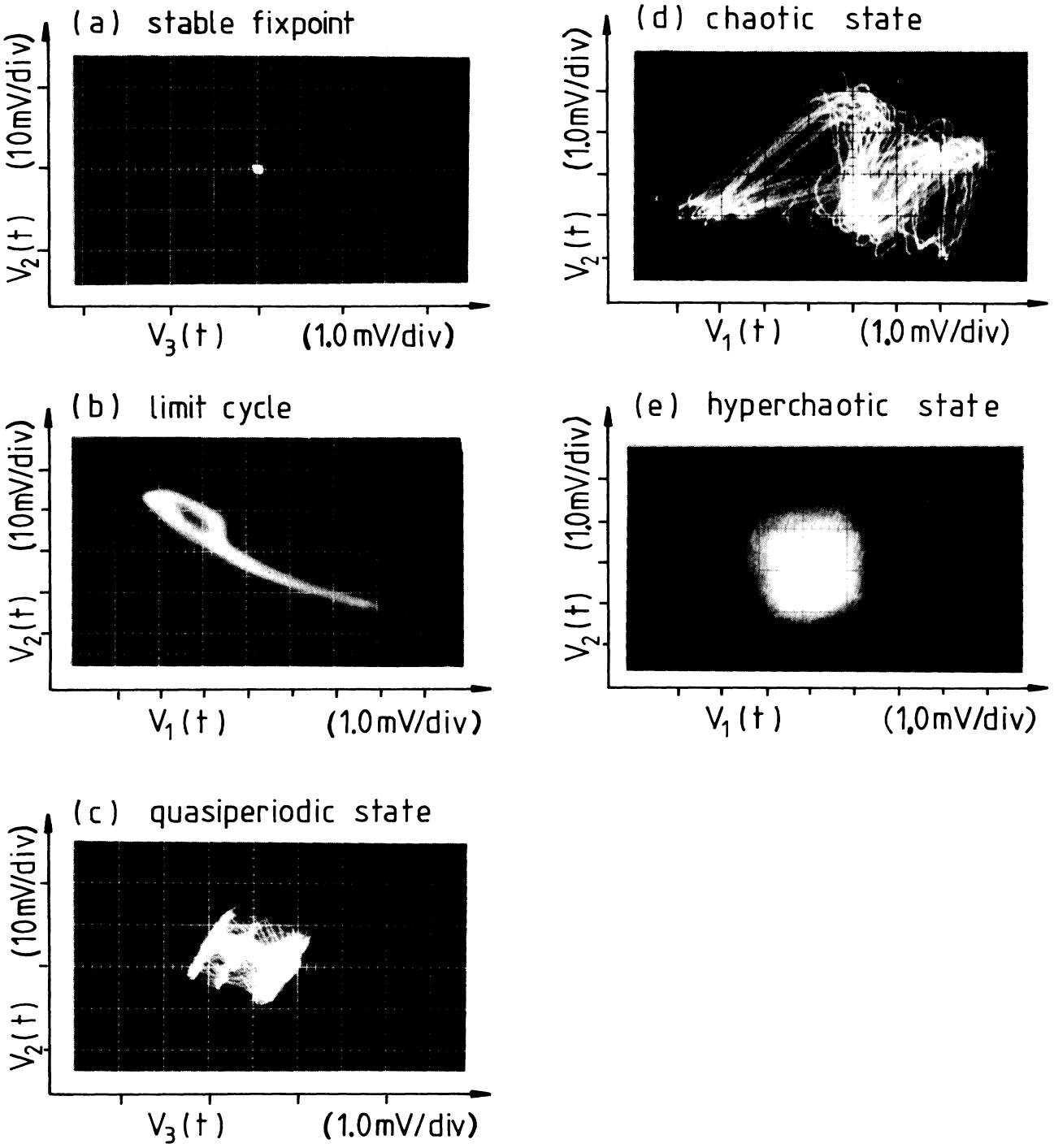

FIG. 2. Phase portraits for distinct nonoscillatory (a), periodic (b), quasiperiodic (c), chaotic (d), and hyperchaotic (e) oscillatory states obtained from the experimental setup sketched in Fig. 1 by plotting pairs of partial voltage drops V_i ($i=1,2,3$) versus one another at different sets of parameter values: (a) bias voltage $V_0=2.220$ V, transverse magnetic field $B=-0.4$ mT, and temperature $T_b=4.2$ K (load resistance $R_L=100\ \Omega$); (b) $V_0=2.184$ V, $B=0$ mT, and $T_b=4.2$ K ($R_L=100\ \Omega$); (c) $V_0=2.220$ V, $B=0.21$ mT, and $T_b=4.2$ K ($R_L=100\ \Omega$); (d) $V_0=2.145$ V, $B=3.15$ mT, and $T_b=4.2$ K ($R_L=100\ \Omega$); (e) $V_0=2.145$ V, $B=4.65$ mT, and $T_b=4.2$ K ($R_L=100\ \Omega$).

its slope only refers to the signal polarity used for presentation. In the case of hyperchaos, no order can be recognized any more. The phase portrait [Fig. 2(e)] displays trajectories running into all directions. Hence, one partial voltage may increase, decrease, or stay constant, while the other changes in one way. That is, both signals develop totally independently from one another in time. Compared to the hyperchaotic behavior, the phase portrait of the chaotic state [Fig. 2(d)] still indicates some measure of correlation among the corresponding two sample parts. It may be worth noting that the numerical analysis of those partial voltage signals with respect to their fractal dimension and their Lyapunov exponents yielded no significant differences among each other.[7] So far, we conclude that there exists a close connection between structural changes in phase space and that in the number of independent variables. The apparent loss of spatial coherence among different sample parts indicates the breakup of our multicomponent semiconductor system from strongly coupled into more independent subsystems (the partial voltages V_i become more independent). In this way, new actively participating degrees of freedom are gained gradually.

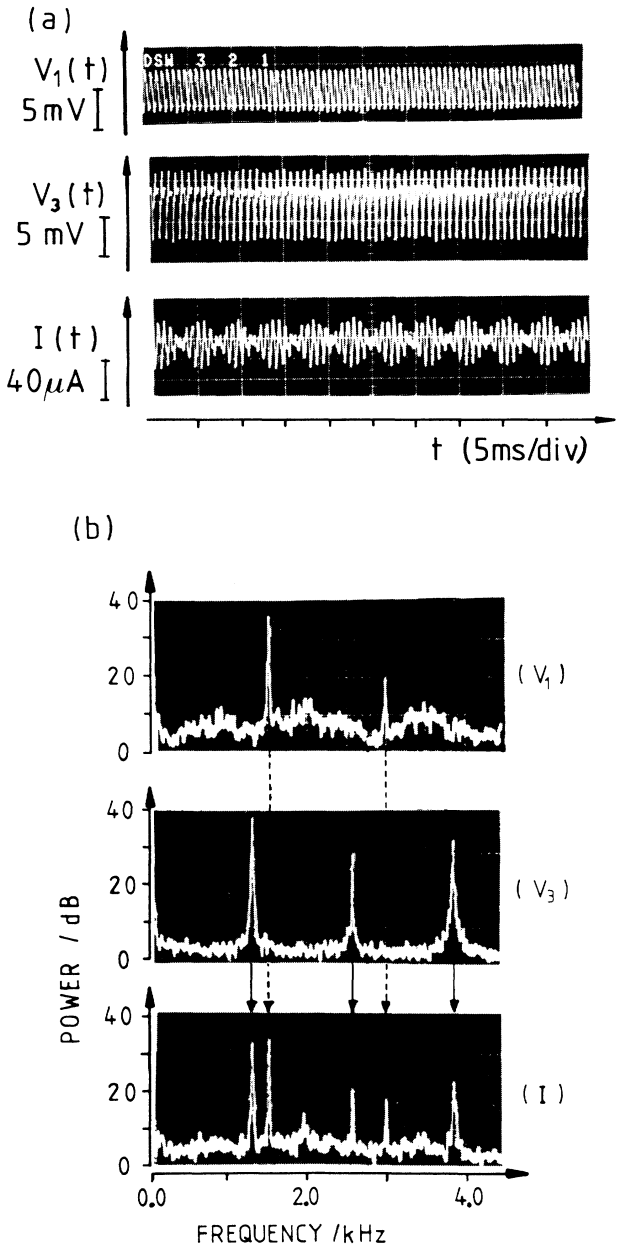

FIG. 3. Temporal profiles (a) and power spectra (b) for a quasiperiodic oscillatory state obtained from the partial voltage drops $V_1(t)$ and $V_3(t)$ and the current signal $I(t)$ according to the experimental setup sketched in Fig. 1 at the constant parameters bias current $I=0.811$ mA, transverse magnetic field $B=0.722$ mT, and temperature $T_b=1.975$ K.

The simplest access to the prevailing spatiotemporal dynamics can be achieved by looking at the quasiperiodic state. As is well known, its description at least requires three independent system variables. Then, one may already observe some typical nonlinear effects. On the other hand, quasiperiodicity is very easily demonstrated by means of a spatial structure embracing two localized oscillators. Figure 3 shows the measurement for a specially chosen parameter set where the simultaneous presence of two competing oscillation centers inside one semiconductor sample could be verified directly. There, the different time traces of the partial voltages V_1 and V_3 together with that of the integral current I are plotted in Fig. 3(a). The power spectra related to these signals can be found in Fig. 3(b). Both the time traces and the power spectra of the partial voltage drops bear witness to almost perfect periodic oscillations distinguished by different frequencies, whereas the current clearly displays quasiperiodic behavior. The arrows drawn in between the power spectra plainly indicate that the current signal reflecting two apparently incommensurate frequencies and their harmonics is composed of two portions originating from the partial voltage drops. These experimental findings give rise to the interpretation that quasiperiodic current flow may derive from the localized periodic oscillatory behavior of at least two spatially separated sample parts. Such spontaneous pattern-forming processes are commonly denoted as synergetic spatiotemporal dynamics that arise in a self-organized way inside the system considered (i.e., without being favored by external excitations or inhomogeneous boundary conditions).

IV. DYNAMICS OF SINGULARIZED SUBSYSTEMS

Next, we present further striking evidence that there are localized oscillation centers by applying the voltage bias only over part of the sample. A possible experimental setup is sketched in Fig. 4. Provided that we have an oscillation center only due to the local conditions of the sample, its dynamical behavior should also be observable when just focusing our investigations solely to the corresponding semiconductor region. On the other side, if the local dynamics results from an interaction of this part with the whole sample, a somewhat different behavior can be expected for the present experimental situation. In the following, we discuss these ideas along distinct ex-

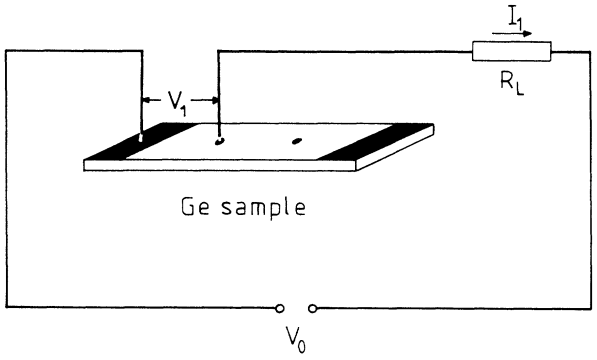

FIG. 4. Scheme of a particular experimental arrangement deviating from that in Fig. 1 by only biasing part 1 of the sample.

perimental findings.

First, the problem arises as to what the appropriate control parameters to ensure that a specific part of the sample is forced to identical working conditions under the different experimental situations outlined in Figs. 1 and 4 are. Of course, the magnetic field and the temperature do not raise any difficulties. For the case of electric conditions such as the bias voltage, the load resistance, and the current, it has turned out satisfactorily that the time-averaged current flow I (also called the bias current) represents the best parameter. Keep in mind that the current will be labeled by I_i or I_{ij}, if application of the bias voltage V_0 is restricted to the sample part i or even the sample parts i and j $(i,j=1,2,3)$, respectively. The corresponding partial voltages V_{ij} are specified accordingly. Take note of the fact that the time-averaged current in any case must flow through the semiconductor sample, no matter how large the resistances of the ohmic contacts are, whereas the voltages can be affected sensitively by different contact resistances.

We start with the discussion of measurements performed during a periodic state of our experimental system. Figures 5(a)–5(d) provide the time signals $I(t)$, $V_1(t)$, $V_2(t)$, and $V_3(t)$, respectively, obtained for supplying the whole sample arrangement with the bias voltage (cf. Fig. 1). It is clearly evident that the periodic oscillation can be detected mainly inside the sample parts 1 and 2. For comparison, Figs. 5(e)–5(h) bring face to face

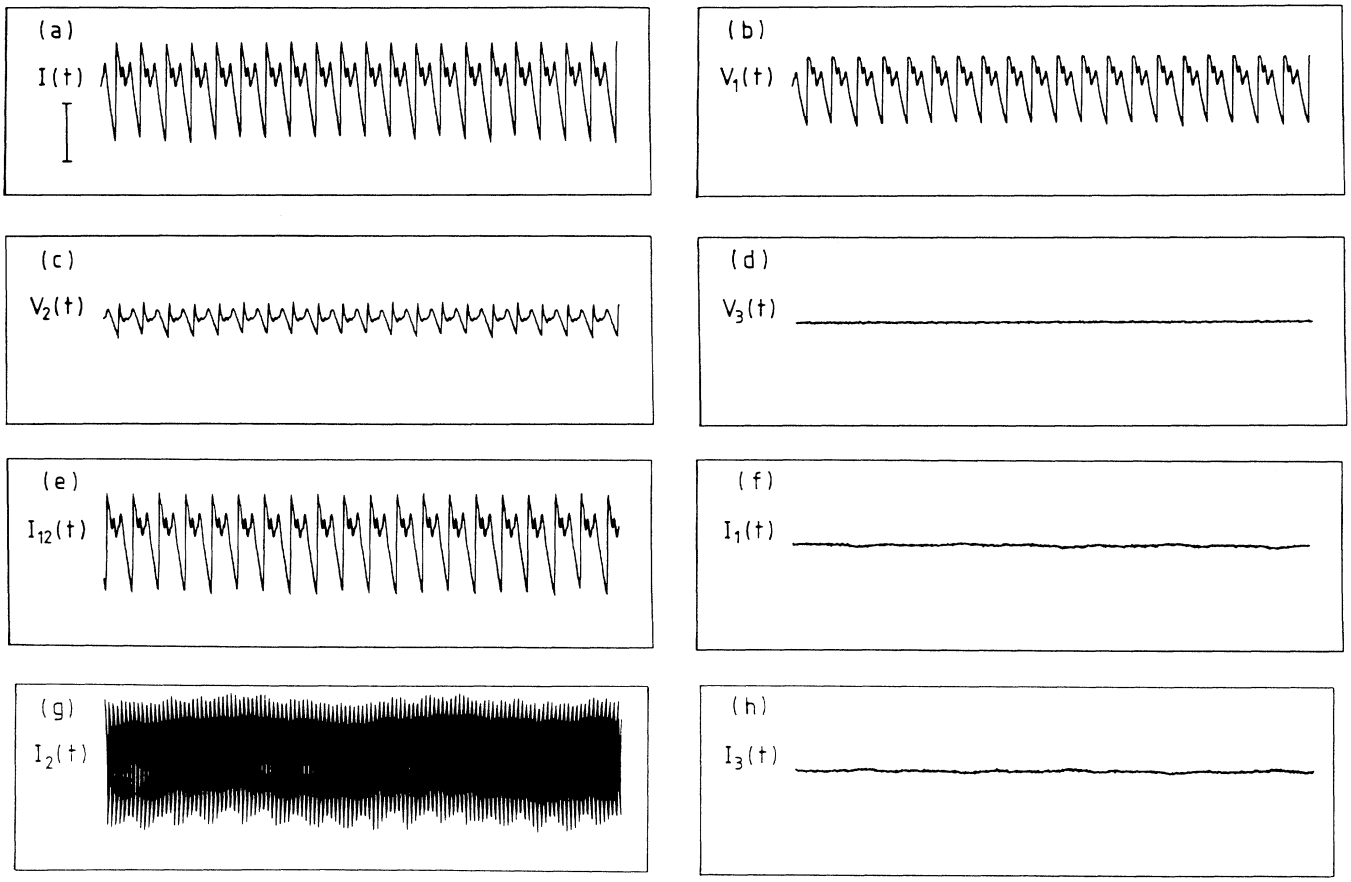

FIG. 5. Temporal current and voltage profiles for two corresponding periodic oscillatory states obtained from the experimental setups sketched in Figs. 1 and 4 by biasing either the whole [(a)–(d)] or different parts [(e)–(h)] of the sample arrangement, respectiveat the constant parameters bias current $I=3.2004\pm0.0002$ mA, transverse magnetic field $B=0.171$ mT, and temperature $T_b=1.98$ K. All signals are plotted on the same vertical and horizontal scale. Their amplitude refers to the 2.5-mV voltage bar indicated in (a). The current was measured as voltage drop at a 10-kΩ load resistor. The total time span amounts to 50 ms.

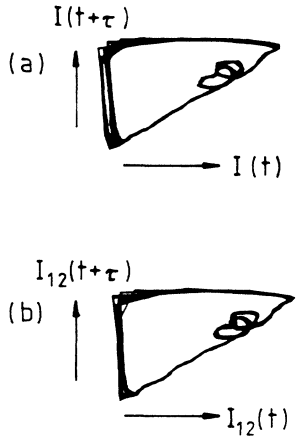

FIG. 6. Phase portraits for the case of the two corresponding periodic oscillatory states in Fig. 5 (same sample and control parameters) obtained from the current signals $I(t)$ and $I_{12}(t)$ using a delay time of 100 μs.

the corresponding time signals $I_{12}(t)$, $I_1(t)$, $I_2(t)$, and $I_3(t)$, respectively, obtained for separately biasing different sample parts (cf. Fig. 4). Only in case of the arrangement investigating part 1 together with part 2, there results a periodic signal $I_{12}(t)$ similar to $I(t)$. The almost identical shape of the corresponding phase portraits in Fig. 6 reconstructed from the time series of the currents I (a) and I_{12} (b) gives rise to the conclusion that in the state considered the total system dynamics is located inside sample parts 1 and 2. Further support can be extracted from the magnetic field dependence of the frequency of those current signals, displayed in Fig. 7. The frequency scaling detected is characteristic for one generic bifurcation from a fixed point to a limit cycle.[2,20] Keeping in mind that bifurcations are highly sensitive against smallest changes of the boundary conditions, we can take the results of Fig. 7 as proof that the local dynamics of sample part 3 does not contribute to the prevailing periodic state. In other words, it would be possible to cut off part 3 from the sample configuration without examining any influence on the overall dynamics. However, dividing up the sample into further subregions

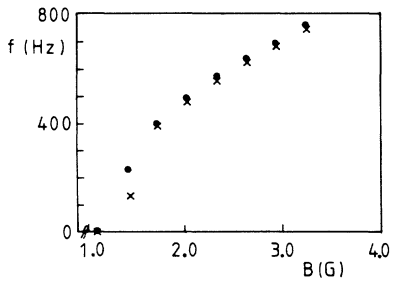

FIG. 7. Dependence of the frequency upon the transverse magnetic field (1 G≙0.1 mT) for the case of the two corresponding periodic oscillatory states of the currents I and I_{12} (marked by dots and crosses, respectively) in Fig. 5 (same sample and constant parameters).

(i.e., parts 1 and 2), one receives a different type of dynamics, obviously not any more correlated with the former one [compare the signals $I_2(t)$ and $V_2(t)$ in Fig. 5]. Not least this finding confirms our notion that the periodic current signal $I(t)$ in Fig. 5 derives from the interaction of oscillatory subsystems that are located in parts 1 and 2 of the sample. This phenomenon can be set in direct analogy to collective synchronization of subsystems.[1] For the present semiconductor experiment, the appropriate model approach seems to proceed from a hierarchical ordering of subsystems that create clusters of spatially homogeneous dynamics. These clusters then, in turn, represent nothing but mutually interacting subsystems capable to form further cluster configurations. We point out that the size of the smallest oscillatory unit observed experimentally was in the range of 10 μm.[13]

V. DYNAMICS OF COUPLED SUBSYSTEMS

A second example of spatiotemporal behavior concerns the quasiperiodic state to be presented in the following. Analogous to the previous results of Fig. 3, quasiperiodicity in the current signal $I(t)$ of Fig. 8(a) can be attributed to the superposition of the two nearly periodic voltage traces $V_{12}(t)$ and $V_3(t)$ shown in Figs. 8(b) and 8(c), respectively. Since all three time signals were digitized synchronously, the modulation of the amplitude of $V_{12}(t)$ is found to be highly correlated with the periodicity of $V_3(t)$. The current signals $I_{12}(t)$ and $I_3(t)$ that correspond to these partial voltages (accordingly measured at separate bias control of the sample parts under consideration) are plotted in Figs. 8(d) and 8(e), respectively. Juxtaposition of $V_{12}(t)$ and $I_{12}(t)$ yields very similar time traces; even their frequencies coincide within an experimental inaccuracy of some percent. If one compares $V_3(t)$ with $I_3(t)$, again reasonable agreement in the shape of both signals can be recognized, while the frequency of the latter noticeably is higher. So far, these findings prove this quasiperiodic state to arise from two competing oscillation centers located in spatially separated parts of the semiconductor. One oscillator is localized inside the region that embraces parts 1 and 2, the other inside part 3 of the sample. An important result was that those localized oscillation centers could be activated independently from each other only by addressing the voltage bias to the distinct sample part coming into question.

The characteristic magnetic-field dependence of the frequency components involved gives prominence to the mutual relationship between one oscillation and the other. Figure 9(a) displays the successive development of two independent frequencies in the case of applying the experimental setup of Fig. 1. The bifurcation to a quasiperiodic state takes place at a transverse magnetic field of slightly above 0.4 mT. The plot in the inset shows the square-root scaling of the second frequency with the magnetic field close to the bifurcation point, a characteristic of this bifurcation.[2,20] On the other hand, Figs. 9(b) and 9(c) unveil the relating frequency behavior for the two particular arrangements of separately biasing different parts of the sample (cf. Fig. 4). In accordance with the conclusions drawn from the time signals in Fig. 8, the

graph of the first intrinsic frequency in Fig. 9(a) and that of the single frequency in Fig. 9(b) are almost identical. There is only little difference at the jump down to lower frequencies around 0.7 mT. Pronounced deviations can be found, if one compares the behavior of the second intrinsic frequency in Fig. 9(a) with that of the single frequency in Fig. 9(c). Two features become immediately evident. First, the bifurcation point in situation (a) is shifted to higher magnetic fields such that all frequency values are generally smaller—with respect to the magnetic field applied—than the corresponding ones in situation

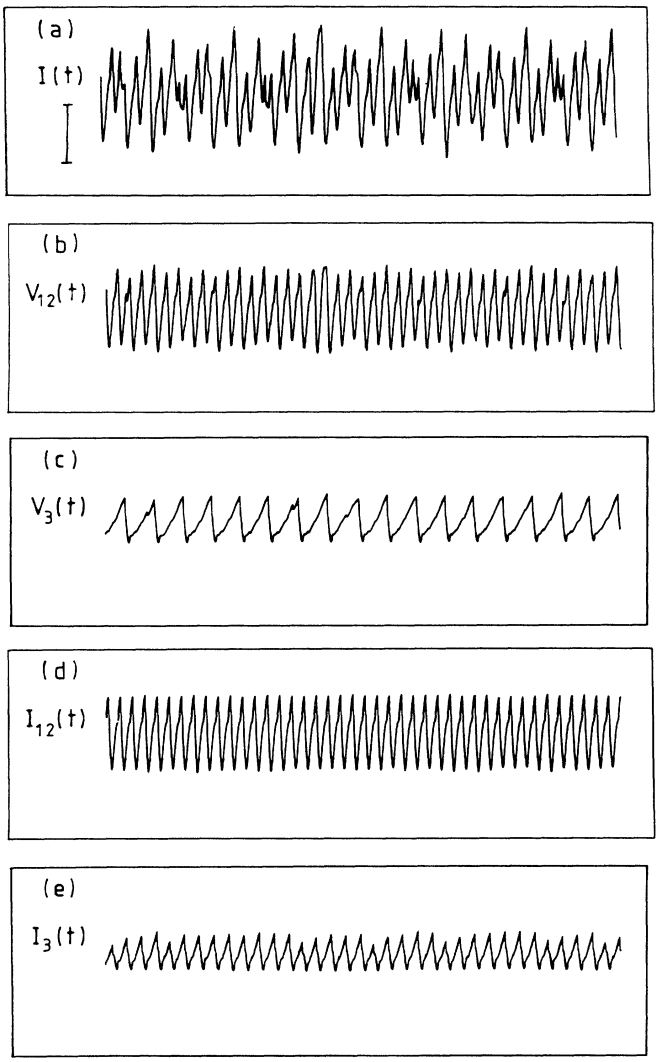

FIG. 8. Temporal current and voltage profiles for two corresponding periodic and quasiperiodic oscillatory states obtained from the experimental setups sketched in Figs. 1 and 4 by biasing either the whole [(a)–(c)] or different parts [(d) and (e)] of the sample arrangement, respectively, at the constant parameters bias current $I=2.284\pm0.001$ mA, transverse magnetic field $B=0.506$ mT, and temperature $T_b=2.10$ K. All signals are plotted on the same vertical and horizontal scale. Their amplitude refers to the 5-mV voltage bar indicated in (a). The current was measured as voltage drop at a 10-kΩ load resistor. The total time span amounts to 33 ms.

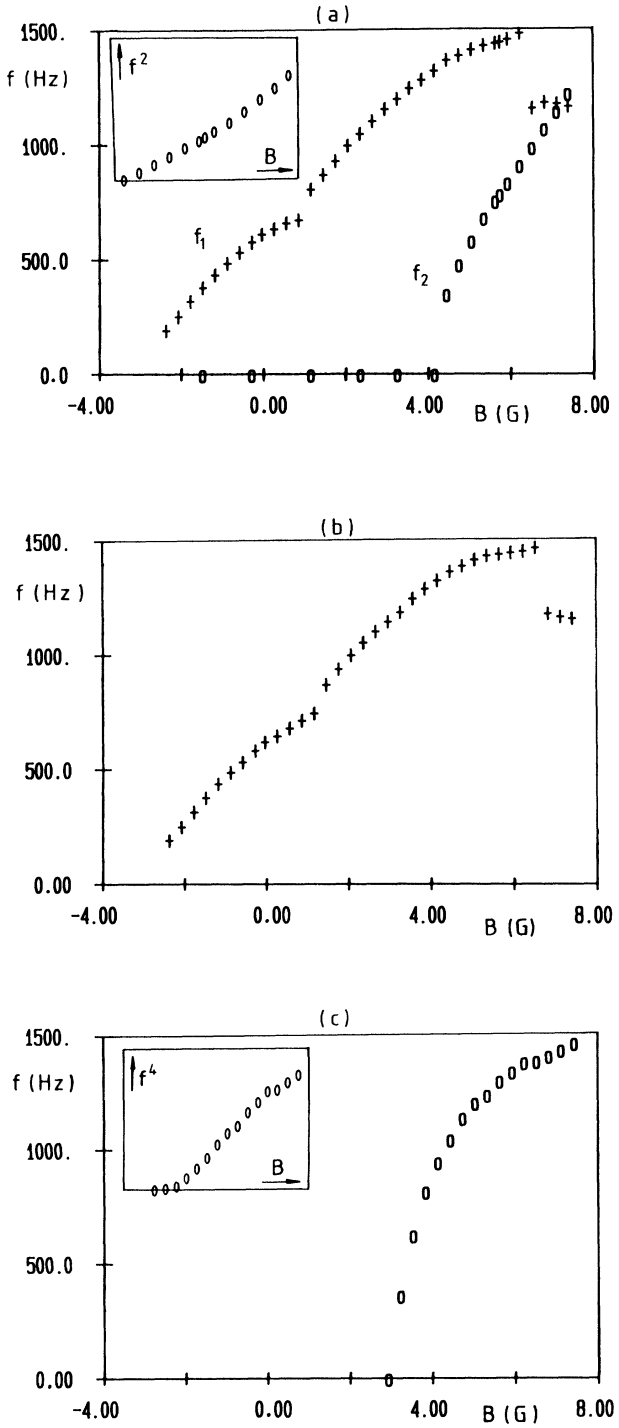

FIG. 9. Dependence of the intrinsic frequencies upon the transverse magnetic field (1 G≙0.1 mT) for the case of the two corresponding periodic and quasiperiodic oscillatory states of the currents I (a), I_{12} (b), and I_3 (c) in Fig. 8 (same sample and constant parameters). The data of the two frequencies f_1 and f_2 existing simultaneously in the current signal $I(t)$ as well as the corresponding single frequencies of the current signals $I_{12}(t)$ and $I_3(t)$ are marked by crosses and circles, respectively. The insets in (a) and (c) appreciate the scaling of the (circle) frequency data near the bifurcation point.

(c). Second, the power law of the scaling in the vicinity of the bifurcation point changes from the exponent 1/2 in situation (a) to the exponent 1/4 in situation (c), as indicated by particular plots in the relating figure insets. Apparently, the interaction between the two oscillation centers manifests in the way that the presence of the first intrinsic system frequency (say, f_1) can prevent the appearance of the second one (say, f_2) over an extended control parameter interval. This finding is clearly different from that expected for a driven damped oscillator. In the latter case, the damped oscillator becomes activated due to the interaction with the external driving force.

A similarly unambiguous signature for the existence of a nonlinear coupling between the oscillators can be provided by looking at the existence of mode locking phenomena. In a quasiperiodic scenario, such a kind of dynamics represents an important step towards the onset of chaos, as demonstrated elsewhere for the case of the present semiconductor system.[21,22] Upon analyzing more thoroughly the frequency scaling behavior of the whole sample arrangement in Fig. 9, we disclose the 1/2 and 1/1 locking states at the magnetic-field parameter values $B=0.55$ mT and $B=0.72$ mT, respectively. Experimental evidence of the latter case is illustrated in Fig. 10 by plotting the control parameter dependence of the difference $\Delta f=f_1-f_2$ between the two existing frequencies f_1 and f_2. Obviously, the 1/1 locking region with $\Delta f=0$ extends over a finite magnetic-field range of 0.006 mT. The 1/2 locking state was found to cover about 0.005 mT (not shown here). If one readily carries forward those findings to that obtained from investigating only parts of the sample arrangement (see Fig. 9), there appear considerable deviations in the frequency difference of the corresponding locking states.

Another experimental point of view concerns the spatiotemporal aspects underlying a quasiperiodic state, where the power spectrum is dominated by protruding frequency mixing components. They provide a further proof for the presence of a nonlinear interaction between the intrinsic oscillatory modes. Figures 11(a)–11(c) give the power spectrum of the integral current signal $I(t)$ together with that of the partial voltage drops $V_{12}(t)$ and $V_3(t)$, respectively, obtained for applying the bias voltage to the whole sample arrangement (cf. Fig. 1). The different spectral peaks are distinguished by the indices (n,m) according to the frequency notation $f=nf_1+mf_2$. There is no doubt that all three power spectra contain mixing components of the two fundamental frequencies f_1 and f_2. Upon separating both oscillation centers via independent bias application to the relating sample regions (cf. Fig. 4), the power spectra of the resulting integral current flow $I_{12}(t)$ and $I_3(t)$ displayed in Figs. 11(d) and 11(e), respectively, do not continue exhibiting any mixing component. Hence, the nonlinear coupling has been clearly switched off. Moreover, in both cases remaining single frequencies are shifted to slightly different values. The lower frequency f_1 decreases further by 125 Hz, while the higher frequency f_2 increases by 62 Hz. We draw the conclusion that the interaction of both oscillation centers, which can take place only when applying the experimental setup in Fig. 1, causes the two fundamental frequencies to attract each other.

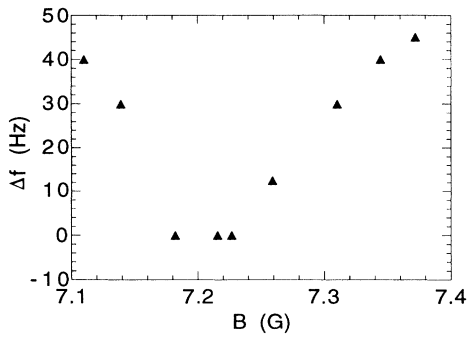

FIG. 10. Dependence of the difference between the two intrinsic frequencies upon the transverse magnetic field (1 G ≙ 0.1 mT) for the case of the 1/1 locking oscillatory state of the current I in Fig. 9 (same sample and constant parameters).

Finally, we extend our analysis from the spatiotemporal dynamics of regular periodic and quasiperiodic states to that of the more complex cases of ordinary chaos and hyperchaos, the phase portraits of which are outlined in Figs. 2(d) and 2(e), respectively. As we have already mentioned above, no significant differences in the diverse chaotic properties (like, e.g., fractal dimensions and Lyapunov exponents) were found if one investigates either the integral current flow or the partial voltage drops in the whole sample arrangement (cf. Fig. 1). Nevertheless, the phase portraits constructed from plotting different partial voltages versus one another clearly indicate loss of spatial coherence. The phenomenon will be quantified numerically as follows.

In order to evaluate the degree of spatial correlation, we have adapted a recently proposed method[23] to the present situation of chaotic and hyperchaotic dynamics.[24] Compared with standard correlation measurements, the above procedure has been demonstrated to excel by serious advantages, i.e., extremely fast convergence properties and the feasibility of capturing nonsymmetric relations. The basic idea is that two simultaneously recorded signals, $x(t)=(x_1,\ldots,x_N)$ and $y(t)=(y_1,\ldots,y_N)$, are interrelated if for one signal (say, x) two points x_i^M and x_j^M in the reconstructed M-dimensional phase space lie inside an ε neighborhood. It follows for the other signal (say, y) that $|y_i^M-y_j^M|$ depends on ε. In contrast, if $|y_i^M-y_j^M|$ is independent of ε, we take $x(t)$ and $y(t)$ as being not interrelated. The M-dimensional points in phase space are defined as $x_i^M=M^{-1/2}(x_i,\ldots,x_{i+M-1})$ and $y_i^M=M^{-1/2}(y_i,\ldots,y_{i+M-1})$. Their ε interrelation can be expressed by the mean conditional dispersion

$$\sigma_{xy}^M=\left[\frac{\sum_{i\neq j}|y_i^M-y_j^M|^2\Theta(\varepsilon-|x_i^M-x_j^M|)}{\sum_{i\neq j}\Theta(\varepsilon-|x_i^M-x_j^M|)}\right]^{1/2}, \quad (1)$$

where Θ denotes the Heaviside function. The conditional

dispersion depends on M and ε. For large M, we have convergence against a limiting curve. At large ε, it is a constant, i.e., independent of ε. Upon decreasing ε, a transition to the regime of ε dependence takes place.[24] The transition point ε_0^M marks the onset of ε dependence of σ_{xy}^M and, thus, the interrelation of the signals x and y, given by

$$K_{xy} = \lim_{M\to\infty} \varepsilon_0^M/\varepsilon_{\max}^M . \tag{2}$$

Here, the normalizing value $\varepsilon_{\max}^M$ is just the size of the attractor.

In Fig. 12, we present the numerical results obtained for the case of the interrelation coefficients K_{12} and K_{21} (with indices 1 and 2 corresponding to the voltage signals V_1 and V_2, respectively). Hereto, the partial voltages V_1 and V_2 were digitized simultaneously (each time 100 000 data points). In order to characterize the development of the spatial interrelation coefficients as the system transits from chaos to hyperchaos, we have employed five different control parameter values. It can be clearly seen how the interrelation is affected during the transition between the two dynamical states. First, a pronounced decrease of the interrelation coefficients accentuates the transition onset. Second, there exists a strong asymmetry in K_{12} and K_{21}. We conclude that the transition between the different chaotic states is closely related to structural changes in space.

At last, we point out that investigating only parts of the sample arrangement (cf. Fig. 4) did not unveil further new insight—in contrast to the intriguing results of the periodic and quasiperiodic states. In the case of higher-dimensional dynamics, both chaotic and hyperchaotic states reflect a totally different spatiotemporal behavior in

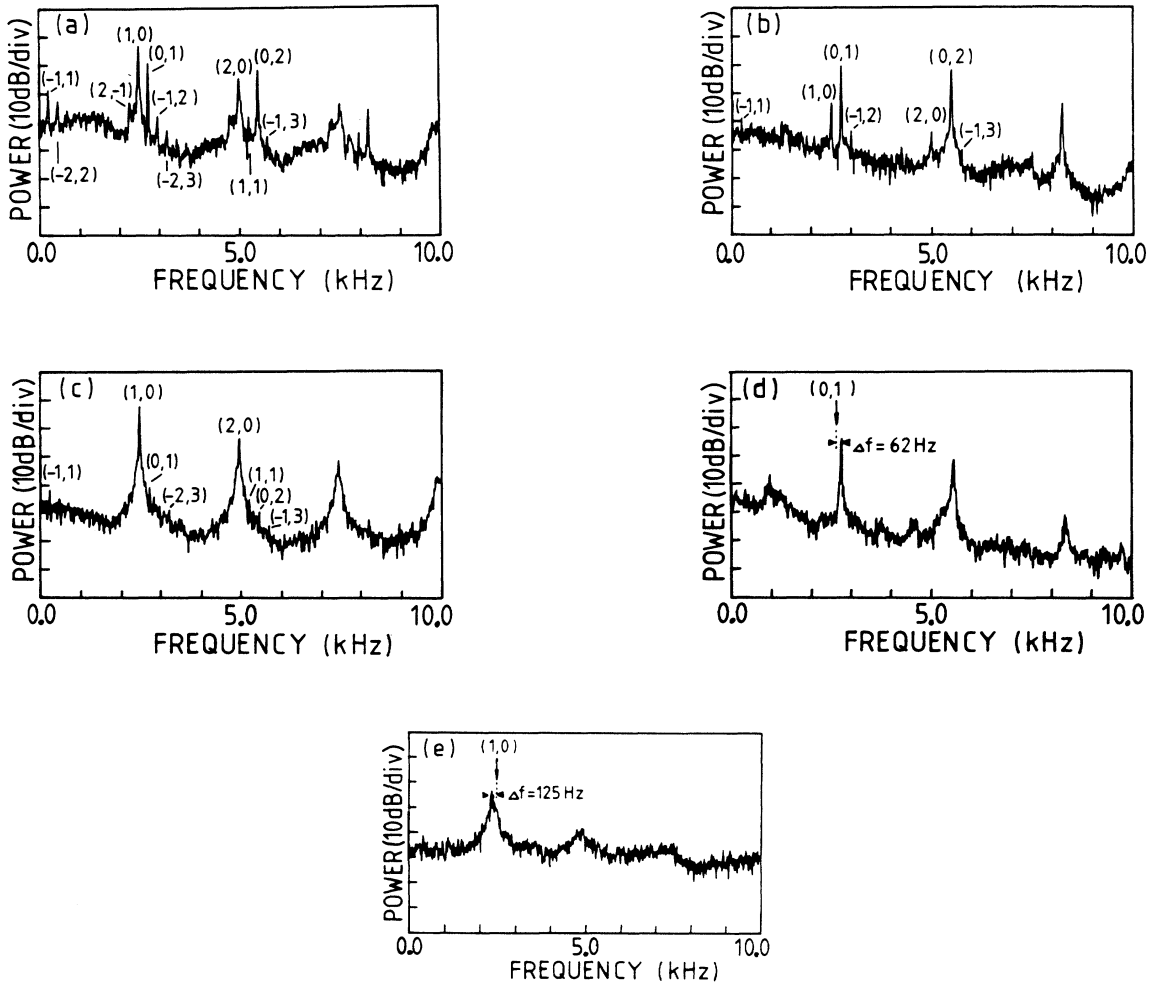

FIG. 11. Power spectra for two corresponding periodic and quasiperiodic oscillatory states of the currents and voltages I (a), V_{12} (b), V_3 (c), I_{12} (d), and I_3 (e) obtained from the experimental setups sketched in Figs. 1 and 4 by biasing either the whole [(a)–(c)] or different parts [(d) and (e)] of the sample arrangement, respectively, at the constant parameters bias current $I = 1.774 \pm 0.001$ mA, transverse magnetic field $B = 0.225$ mT, and temperature $T_b = 2.10$ K. The spectral lines labeled by (n,m) are subject to the frequency $f = nf_1 + mf_2$. The differences of the two frequencies f_1 and f_2 existing simultaneously in the current and voltage signals $I(t)$, $V_{12}(t)$, and $V_3(t)$ to the corresponding single frequencies of the current signals $I_{12}(t)$ and $I_3(t)$ are indicated by Δf in (d) and (e).

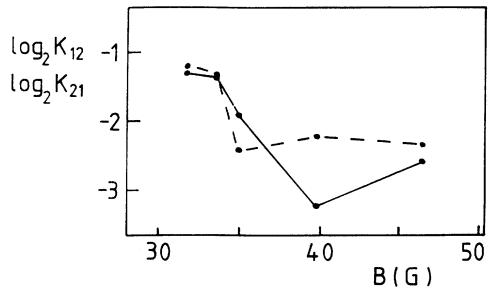

FIG. 12. Dependence of the spatial interrelation coefficients upon the transverse magnetic field (1 G $\hat{=}$0.1 mT) for the case of the transition from the chaotic to the hyperchaotic oscillatory state in Fig. 2 (same sample and constant parameters). The coefficients K_{12} and K_{21} are distinguished by the dashed and solid curve, respectively.

the various partial voltage drops, particularly with respect to signal amplitudes and typical revolution times.

VI. CONCLUSION

We have disclosed several striking indications that the emergence of spontaneous oscillations in our semiconductor system must be closely linked to the spatial formation of localized oscillation centers. The observation of different dynamical states obeying a hierarchical order of complexity is, therefore, a pure consequence of gradual rearrangements among distinct spatiotemporal transport structures in low-dimensional phase space. On the one hand, the spatially separated oscillatory subsystems develop in a self-organized way, i.e., without being favored by external periodic excitations or boundary conditions. On the other hand, the mutual interaction between these oscillators can be sensitively influenced by the help of appropriate control parameters. Such a picture of a coupled multicomponent synergetic system creating the spatiotemporal dynamics measured stands in contrast to a nonlocalized physical mechanism, so far taken as a convenient ansatz for the nonlinear dynamical behavior of various semiconductor experiments.

ACKNOWLEDGMENTS

The authors wish to thank K. Aoki, A. Cenys, W. Clauss, R. P. Huebener, A. Kittel, G. Lasiene, K. Pyragas, U. Rau, O. E. Rössler, and R. Stoop for numerous discussions and the Volkswagen-Stiftung for financial support in part.

[1] *Proceedings of the Workshop on Spatio-Temporal Coherence and Chaos in Physical Systems, Los Alamos, 1986* (North-Holland, Amsterdam, 1986), edited by A. R. Bishop, G. Gruener, and B. Niclaenko [Physica D **23**, (1986)]; P. Keller and M. Duong-van, Nucl. Phys. B **2**, (Proc. Suppl.) 603 (1987); K. Kaneko, Phys. Lett. A **125**, 25 (1987); Europhys. Lett. **6**, 193 (1987); Physica D **34**, 1 (1989); P. C. Matthews and S. H. Strogatz, Phys. Rev. Lett. **65**, 1701 (1990); H. Chate and P. Manneville, Europhys. Lett. **14**, 409 (1991).

[2] J. Peinke, U. Rau, W. Clauss, R. Richter, and J. Parisi, Europhys. Lett. **9**, 743 (1989).

[3] J. Peinke, J. Parisi, U. Rau, W. Clauss, B. Röhricht, R. P. Huebener, and R. Stoop, in *A Chaotic Hierarchy,* edited by G. Baier and M. Klein (World Scientific, Singapore, 1991), p. 317.

[4] J. Peinke, A. Mühlbach, R. P. Huebener, and J. Parisi, Phys. Lett. A **108**, 407 (1985).

[5] J. Peinke, B. Röhricht, A. Mühlbach, J. Parisi, Ch. Nöldeke, R. P. Huebener, and O. E. Rössler, Z. Naturforsch. **40a**, 562 (1985).

[6] R. Richter, J. Peinke, W. Clauss, U. Rau, and J. Parisi, Europhys. Lett. **14**, 1 (1991).

[7] R. Stoop, J. Peinke, J. Parisi, B. Röhricht, and R. P. Huebener, Physica D **35**, 425 (1989).

[8] J. Peinke, A. Mühlbach, B. Röhricht, B. Wessely, J. Mannhart, J. Parisi, and R. P. Huebener, Physica D **23**, 176 (1986).

[9] J. Parisi, J. Peinke, B. Röhricht, U. Rau, M. Klein, and O. E. Rössler, Z. Naturforsch. **42a**, 655 (1987).

[10] K. M. Mayer, R. Gross, J. Parisi, J. Peinke, and R. P. Huebener, Solid State Commun. **63**, 55 (1987).

[11] K. M. Mayer, J. Parisi, J. Peinke, and R. P. Huebener, Physica D **32**, 306 (1988).

[12] K. Aoki, U. Rau, J. Peinke, J. Parisi, and R. P. Huebener, J. Phys. Soc. Jpn. **59**, 420 (1990); U. Rau, K. Aoki, J. Peinke, J. Parisi, W. Clauss, and R. P. Huebener, Z. Phys. B **81**, 53 (1990).

[13] J. Peinke, J. Parisi, B. Röhricht, K. M. Mayer, U. Rau, W. Clauss, R. P. Huebener, G. Jungwirt, and W. Prettl, Appl. Phys. A **48**, 155 (1989).

[14] E. Schöll, *Nonequilibrium Phase Transitions in Semiconductors* (Springer, Berlin, 1987).

[15] W. Clauss, U. Rau, J. Parisi, J. Peinke, R. P. Huebener, H. Leier, and A. Forchel, J. Appl. Phys. **67**, 2980 (1990).

[16] K.-D. Morhard, R. P. Huebener, W. Clauss, and J. Peinke, J. Appl. Phys. **71**, 3336 (1992).

[17] J. Parisi, J. Peinke, U. Rau, and K. M. Mayer, Philos. Mag. Lett. **57**, 311 (1988).

[18] J. Peinke, J. Parisi, O. E. Rössler, and R. Stoop, *Encounter with Chaos* (Springer, Berlin, 1992).

[19] U. Rau, W. Clauss, A. Kittel, M. Lehr, M. Bayerbach, J. Parisi, J. Peinke, and R. P. Huebener, Phys. Rev. B **43**, 2255 (1991).

[20] H. B. Stewart, Z. Naturforsch. **41a**, 1412 (1986).

[21] J. Peinke, J. Parisi, B. Röhricht, B. Wessely, and K. M. Mayer, Z. Naturforsch. **42a**, 841 (1987).

[22] J. Peinke, J. Parisi, R. P. Huebener, M. Duong-van, and P. Keller, Europhys. Lett. **12**, 13 (1990).

[23] A. Cenys, G. Lasiene, and K. Pyragas, Physica D **52**, 332 (1991).

[24] A. Cenys, K. Pyragas, J. Peinke, J. Parisi, R. Richter, and A. Kittel, Phys. Lett. A **164**, 201 (1992).

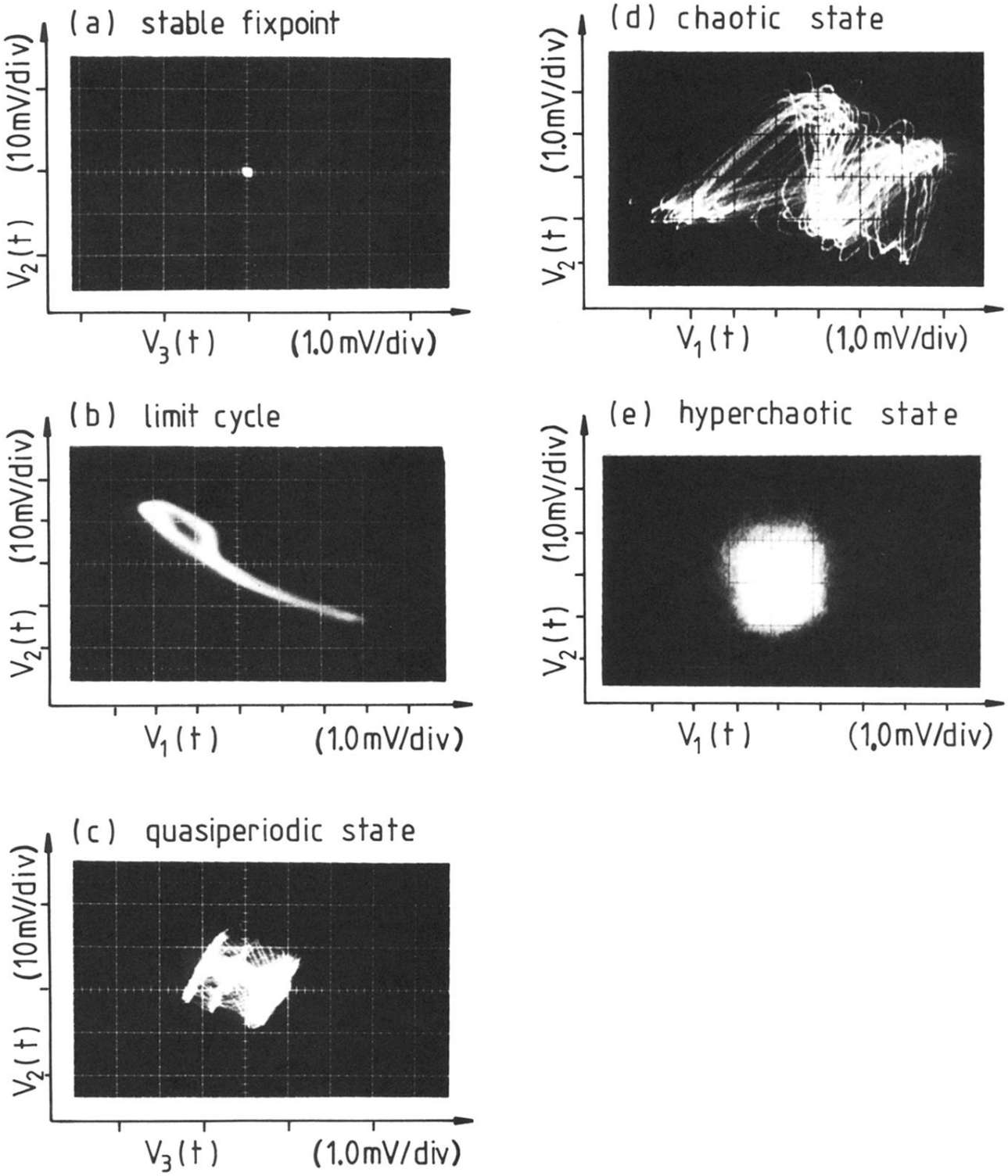

FIG. 2. Phase portraits for distinct nonoscillatory (a), periodic (b), quasiperiodic (c), chaotic (d), and hyperchaotic (e) oscillatory states obtained from the experimental setup sketched in Fig. 1 by plotting pairs of partial voltage drops V_i ($i=1,2,3$) versus one another at different sets of parameter values: (a) bias voltage $V_0=2.220$ V, transverse magnetic field $B=-0.4$ mT, and temperature $T_b=4.2$ K (load resistance $R_L=100\ \Omega$); (b) $V_0=2.184$ V, $B=0$ mT, and $T_b=4.2$ K ($R_L=100\ \Omega$); (c) $V_0=2.220$ V, $B=0.21$ mT, and $T_b=4.2$ K ($R_L=100\ \Omega$); (d) $V_0=2.145$ V, $B=3.15$ mT, and $T_b=4.2$ K ($R_L=100\ \Omega$); (e) $V_0=2.145$ V, $B=4.65$ mT, and $T_b=4.2$ K ($R_L=100\ \Omega$).

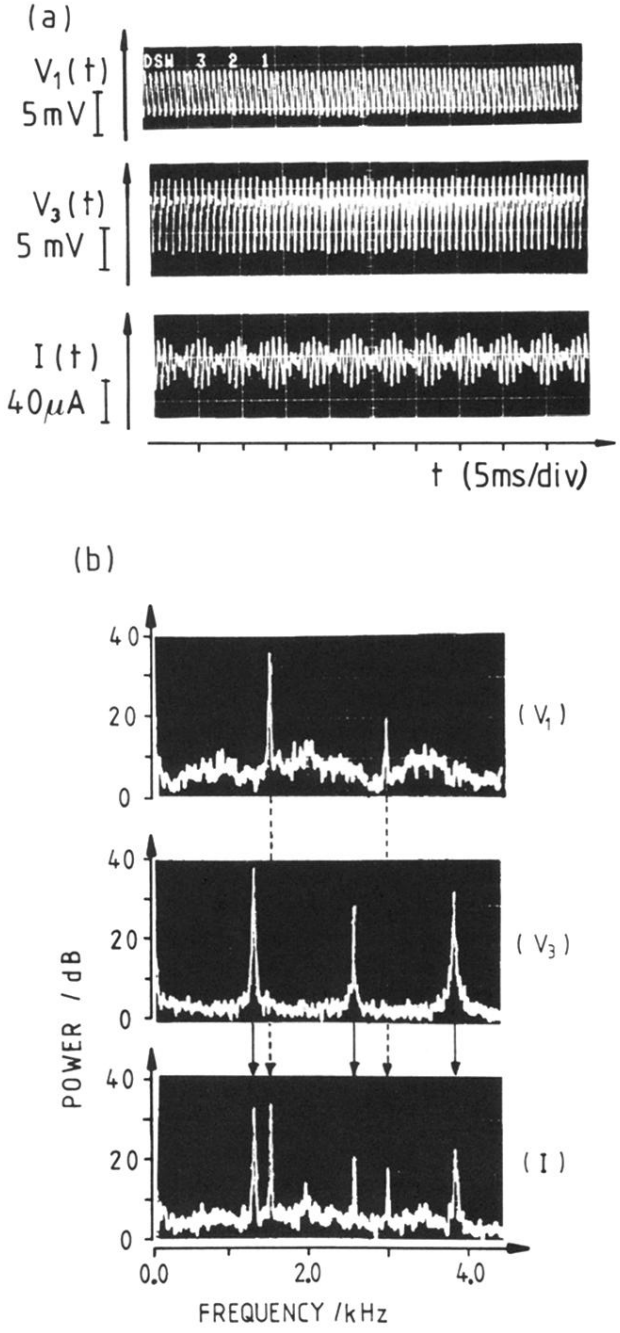

FIG. 3. Temporal profiles (a) and power spectra (b) for a quasiperiodic oscillatory state obtained from the partial voltage drops $V_1(t)$ and $V_3(t)$ and the current signal $I(t)$ according to the experimental setup sketched in Fig. 1 at the constant parameters bias current $I=0.811$ mA, transverse magnetic field $B=0.722$ mT, and temperature $T_b=1.975$ K.